Sc0.43(2)Rb2Mo15S19, a partially Sc-filled variant of Rb2Mo15S19

Patrick Gougeon, Rabih Al Rahal Al Orabi, Régis Gautier, Michel Potel

Acta Crystallographica Section C
Crystal Structure Communications
ISSN 0108-2701

$Sc_{0.43(2)}Rb_2Mo_{15}S_{19}$, a partially Sc-filled variant of $Rb_2Mo_{15}S_{19}$

Patrick Gougeon,[a]* Rabih Al Rahal Al Orabi,[a] Régis Gautier[b] and Michel Potel[a]

[a]Sciences Chimiques de Rennes, CSM–INSA, UMR CNRS No. 6226, Université de Rennes I, Avenue du Général Leclerc, 35042 Rennes CEDEX, France, and [b]Sciences Chimiques de Rennes, UMR CNRS 6226, Ecole Nationale Supérieure de Chimie de Rennes, Avenue du Général Leclerc, CS 50837, 35708 Rennes CEDEX 7, France
Correspondence e-mail: patrick.gougeon@univ-rennes1.fr

Received 29 March 2012
Accepted 16 April 2012
Online 25 April 2012

The structure of scandium dirubidium pentadecamolybdenum nonadecasulfide, $Sc_{0.43\,(2)}Rb_2Mo_{15}S_{19}$, constitutes a partially Sc-filled variant of $Rb_2Mo_{15}S_{19}$ [Picard, Saillard, Gougeon, Noel & Potel (2000), *J. Solid State Chem.* **155**, 417–426]. In the two compounds, which both crystallize in the $R\overline{3}c$ space group, the structural motif is characterized by a mixture of $Mo_6S^i{}_8S^a{}_6$ and $Mo_9S^i{}_{11}S^a{}_6$ cluster units ('i' is inner and 'a' is apical) in a 1:1 ratio. The two components are interconnected through interunit Mo—S bonds. The cluster units are centred at Wyckoff positions 6*b* and 6*a* (point-group symmetries $\overline{3}$. and 32, respectively). The Rb^+ cations occupy large voids between the different cluster units. The Rb and the two inner S atoms lie on sites with 3. symmetry (Wyckoff site 12*c*), and the Mo and S atoms of the median plane of the $Mo_9S_{11}S_6$ cluster unit lie on sites with .2 symmetry (Wyckoff site 18*e*). A unique feature of the structure is a partially filled octahedral Sc site with $\overline{1}$ symmetry. Extended Hückel tight-binding calculations provide an understanding of the variation in the Mo—Mo distances within the Mo clusters induced by the increase in the cationic charge transfer due to the insertion of Sc.

Comment

$In_2Mo_{15}Se_{19}$ (Potel *et al.*, 1981) and $In_3Mo_{15}Se_{19}$ (Grüttner *et al.*, 1979), which crystallize in the $R\overline{3}c$ and $P6_3/m$ space groups, respectively, were the first compounds containing a molybdenum cluster with a nuclearity greater than 6. Indeed, their crystal structures contain an equal mixture of octahedral Mo_6 and bioctahedral Mo_9 clusters. Subsequently, compounds isotypic with $In_2Mo_{15}Se_{19}$, such as $Alc_2Mo_{15}S_{19}$ (Alc = K, Rb or Cs; Picard *et al.*, 2002, 2000, 2004) or $Ba_2Mo_{15}Se_{19}$ (Gougeon *et al.*, 1989), as well as compounds isotypic with $In_3Mo_{15}Se_{19}$, such as $In_{1.6}Rb_2Mo_{15}S_{19}$ and $ScTl_2Mo_{15}S_{19}$ (Salloum *et al.*, 2004), have been obtained. Among the latter compounds, $Rb_2Mo_{15}S_{19}$ appears to be the first member of the series of compounds $Rb_{2n}Mo_9S_{11}Mo_{6n}S_{6n+2}$ (n = 1, 2, 3 and 4; Picard *et al.*, 2000). In addition to their interesting crystal structures, the $Rb_{2n}Mo_9S_{11}Mo_{6n}S_{6n+2}$ compounds become superconducting at low temperature. In an attempt to replace Tl with Rb in $ScTl_2Mo_{15}S_{19}$ ($In_3Mo_{15}Se_{19}$ type), we obtained the title new quaternary compound $Sc_{0.43}Rb_2Mo_{15}S_{19}$ belonging to the $In_2Mo_{15}Se_{19}$ structure type and constituting a partially Sc-filled variant of $Rb_2Mo_{15}S_{19}$.

The insertion of Sc into $Rb_2Mo_{15}S_{19}$ is evident from the variations in the unit-cell parameters: the *a* axis increases by *ca* 0.08 Å, while the *c* axis decreases by about 0.27 Å. A view of the crystal structure of $Sc_{0.43}Rb_2Mo_{15}S_{19}$ is shown in Fig. 1. The Mo—S framework is similar to that of $Rb_2Mo_{15}S_{19}$ and is based on an equal mixture of $Mo_6S^i{}_8S^a{}_6$ and $Mo_9S^i{}_{11}S^a{}_6$ cluster units interconnected through Mo—S bonds (Fig. 2) [for details of the inner ('i') and apical ('a') ligand notation, see Schäfer & von Schnering (1964)]. The first unit can be described as an Mo_6 octahedron surrounded by eight face-capping inner S^i (six S3 and two S5) and six apical S^a (S1) ligands. The Mo_9 core of the second unit results from the face-sharing of two octahedral Mo_6 clusters. The Mo_9 cluster is surrounded by 11 S^i atoms (six S1, three S2 and two S4) capping the faces of the bioctahedron and six apical S^a ligands (S3) above the outer Mo atoms. The $Mo_6S^i{}_8S^a{}_6$ and $Mo_9S^i{}_{11}S^a{}_6$ units are centred at the 6*b* and 6*a*

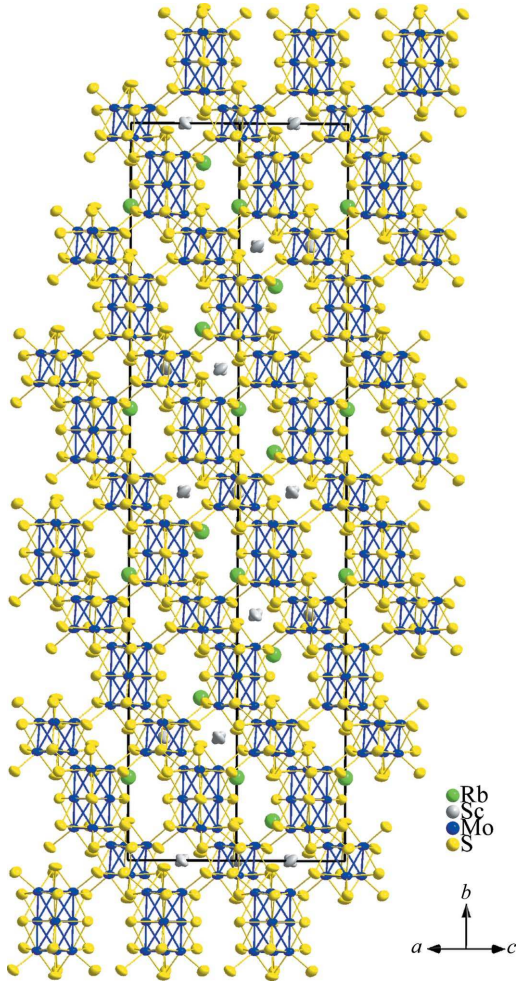

Figure 1
A view of $Sc_{0.43}Rb_2Mo_{15}S_{19}$ along [110].

 doi:10.1107/S0108270112016605

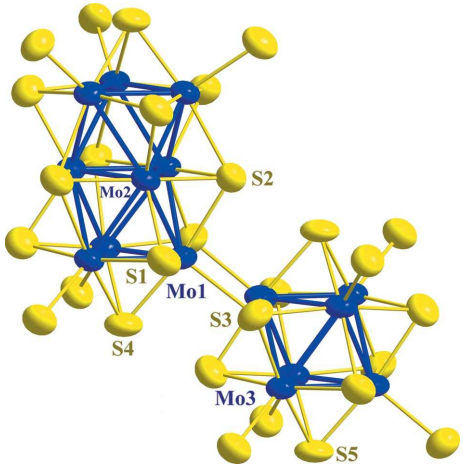

Figure 2
A plot showing the atom-numbering scheme and the inter-unit linkage of the $Mo_9S_{11}S_6$ and $Mo_6S_8S_6$ cluster units. Displacement ellipsoids are drawn at the 97% probability level.

positions and have point-group symmetries $\bar{3}$. and 32, respectively.

The Mo—Mo distances within the Mo_6 clusters are 2.6783 (6) Å for the intratriangle distances (distances within the Mo_3 triangles formed by atoms Mo3 related through the threefold axis) and 2.7393 (6) Å for the intertriangle distances. In $Rb_2Mo_{15}S_{19}$, the latter two values are 2.676 (2) and 2.767 (2) Å, respectively. These variations reflect the different cationic charge transfer towards the Mo_6 clusters in the two parent compounds.

The Mo—Mo distances within the Mo_9 clusters are 2.6658 (5) and 2.6910 (8) Å for the distances in the triangles formed by atoms Mo1 and Mo2, respectively. In $Rb_2Mo_{15}S_{19}$, the corresponding distances are 2.680 (2) and 2.688 (3) Å. The distances between the triangles formed by atoms Mo1 and Mo2 are 2.6958 (4) and 2.7663 (4) Å, respectively, in $Sc_{0.43}Rb_2Mo_{15}S_{19}$, compared with 2.719 (1) and 2.785 (2) Å, respectively, in $Rb_2Mo_{15}S_{19}$.

Although the structural response of the Mo_9 cluster with respect to the increase in charge transfer is more complex, we observe that the Mo1—Mo1 and two Mo1—Mo2 intertriangle distances are shorter in the Sc-filled compound. On the other hand, a slight increase in the Mo2—Mo2 bond distances occurs in the median Mo_3 triangle [2.688 (3) Å in $Rb_2Mo_{15}S_{19}$]. In order to explain these variations, we performed extended Hückel tight-binding (EHTB) calculations on $Rb_2Mo_{15}S_{19}$ using the program *YaEHMOP* (Landrum, 1997). The Mo and S extended Hückel parameters used by Picard *et al.* (2000) were considered. Total Mo_6- and Mo_9-projected DOS (density of states) and COOP (crystal orbital overlap population) curves for the different bonds discussed above and obtained from 36 *k* points of the irreducible wedge of the Brillouin zone are sketched in Figs. 3 and 4, respectively.

Assuming an ionic interaction between the inserted Sc atoms and the host material, the three electrons of the 3*d* transition metal should be transferred to the clusters.

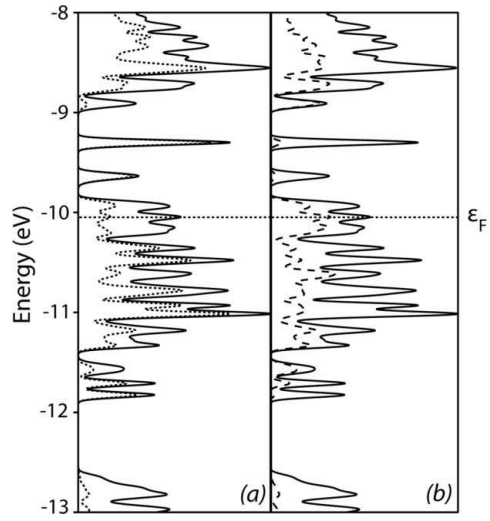

Figure 3
EHTB calculations for $Rb_2Mo_{15}S_{19}$, showing (*a*) total (solid line) and Mo_6-projected (dotted line) DOS, and (*b*) total (solid line) and Mo_9-projected (dotted line) DOS.

Assuming a rigid-band model, the Fermi level corresponding to the electron count of the title compound is slightly higher in energy (*ca* 0.02 eV) than that for $Rb_2Mo_{15}S_{19}$. The DOS at the Fermi level is mainly centred on Mo atoms belonging to both Mo_6 and Mo_9 clusters (Fig. 3). Therefore, both clusters should be affected by an increase in the anionic charge of the Mo–S network. As shown by the COOP curves of the Mo3—Mo3 intratriangle (solid line) and Mo3—Mo3 intertriangle (dotted line) bonds within the Mo_6 cluster, the increase in the metal electron count due to the insertion of Sc foresees a weak lengthening and a shortening of the Mo3—Mo3 bonds within the Mo_3 triangles and between the triangles, respectively. Such an evolution is in fact observed in $Sc_{0.4}Rb_2Mo_{15}S_{19}$, as mentioned above.

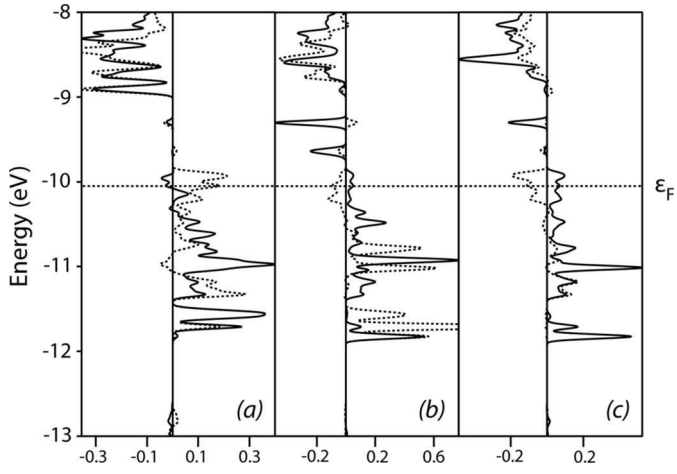

Figure 4
EHTB calculations for $Rb_2Mo_{15}S_{19}$, showing (*a*) Mo3—Mo3 COOPs for interatomic distances within the Mo_3 triangle (solid line) and between triangles (dotted line) of the Mo_6 cluster, (*b*) COOPs for the intratriangle Mo1—Mo1 (solid line) and Mo2—Mo2 (dotted line) bonds in the Mo_9 cluster and (*c*) COOPs for the intertriangle Mo1—Mo2 bonds of 2.719 (solid line) and 2.785 Å (dotted line).

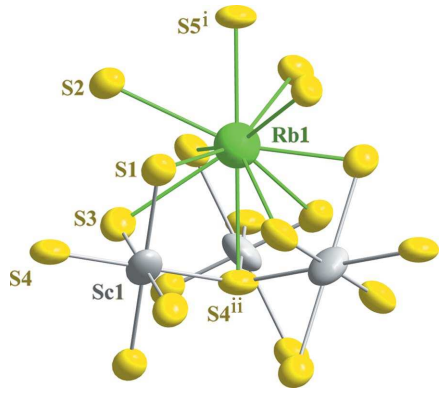

Figure 5
A view of the environment of the Rb^{+} and Sc^{3+} cations. Displacement ellipsoids are drawn at the 97% probability level. Symmetry codes are as in Table 1.

Regarding the Mo_9 cluster (Fig. 4), the lengthening of the Mo2—Mo2 bonds and the shortening of the Mo1—Mo1 and Mo1—Mo2 bonds can be envisioned theoretically when extra electrons are added, and this is what is observed experimentally in $Sc_{0.43}Rb_2Mo_{15}S_{19}$. The Mo—S distances are almost unaffected by the cationic charge, and range between 2.4198 (13) and 2.4736 (10) Å within the $Mo_6S^{i}_{8}S^{a}_{6}$ unit and between 2.4125 (10) and 2.6065 (7) Å within the $Mo_9S^{i}_{11}S^{a}_{6}$ unit, as usual.

Finally, the three-dimensional packing arises from the interconnection of the $Mo_6S^{i}_{8}S^{a}_{6}$ and $Mo_9S^{i}_{11}S^{a}_{6}$ cluster units through Mo—S bonds. Indeed, each $Mo_6S^{i}_{8}S^{a}_{6}$ unit is interconnected to six $Mo_9S^{i}_{11}S^{a}_{6}$ units (and *vice versa*) *via* Mo3—S1 and Mo1—S3 bonds, respectively, to form the three-dimensional Mo–Se framework, the connective formula of which is $Mo_9S^{i}_{5}S^{i\text{-}a}{}_{6/2}S^{a\text{-}i}{}_{6/2}$, $Mo_6S^{i}_{2}S^{i\text{-}a}{}_{6/2}S^{a\text{-}i}{}_{6/2}$. The result of this arrangement is that the shortest intercluster Mo1—Mo3 distance between the Mo_6 and Mo_9 clusters is 3.2995 (4) Å, compared with 3.246 (2) Å in $Rb_2Mo_{15}S_{19}$, indicating only weak metal–metal interaction. This variation is consistent with the Mo–Mo intercluster antibonding nature of the bands that lie in the vicinity of the Fermi level.

The Sc atoms occupy highly flattened octahedral sites [2.1718 (10) (×2), 2.7983 (3) (×2) and 2.9200 (10) Å (×2)] located near the Rb1 sites around the threefold axes. The alkali metal cation occupies a pentacapped trigonal prismatic site of S atoms, similar to that observed in $Rb_2Mo_{15}S_{19}$ (Fig. 5). The Rb—S distances are spread over the wide range 3.2512 (10)–3.7554 (11) Å, while in $Rb_2Mo_{15}S_{19}$ they are in the range 3.222 (3)–3.730 (3) Å. Thus, the insertion of Sc only leads to a slight decrease (*ca* 0.020 Å) of the Rb1—S4 and Rb1—S5 distances along the threefold axis, while the other distances are slightly increased (*ca* 0.027 Å).

Experimental

Single crystals of $Sc_{0.43}Rb_2Mo_{15}S_{19}$ were prepared from a mixture of Sc_2S_3, Rb_2MoS_4, MoS_2 and Mo with the nominal composition $ScRb_2Mo_{15}S_{19}$. Rubidium thiomolybdate was obtained by sulfuration of Rb_2MoO_4 at 723 K for 2 d under CS_2 gas carried by flowing argon. The molybdate Rb_2MoO_4 was synthesized by heating an equimolar ratio of Rb_2CO_3 and MoO_3 in an alumina vessel at 1073 K in air over a period of 2 d. Sc_2S_3 was prepared from the elements heated in a sealed evacuated silica tube at 1073 K for 2 d. All handling of materials was carried out in an argon-filled glove-box. The initial mixture (*ca* 5 g) was cold pressed and loaded into a molybdenum crucible, which was sealed under a low argon pressure using an arc-welding system. The charge was heated at a rate of 300 K h^{-1} to 1773 K and the temperature held for 48 h. The charge was then cooled at a rate of 100 K h^{-1} to 1373 K before being finally furnace cooled.

Crystal data

$Sc_{0.43(2)}Rb_2Mo_{15}S_{19}$
M_r = 2238.37
Trigonal, $R\overline{3}c$
a = 9.5173 (1) Å
c = 56.0061 (9) Å
V = 4393.33 (10) $Å^3$
Z = 6
Mo $K\alpha$ radiation
μ = 10.92 mm^{-1}
T = 293 K
0.13 × 0.12 × 0.09 mm

Data collection

Nonius KappaCCD area-detector diffractometer
Absorption correction: analytical (de Meulenaer & Tompa, 1965)
T_{min} = 0.298, T_{max} = 0.463
13057 measured reflections
1431 independent reflections
1383 reflections with $I > 2\sigma(I)$
R_{int} = 0.069

Refinement

$R[F^2 > 2\sigma(F^2)]$ = 0.029
$wR(F^2)$ = 0.062
S = 1.25
1431 reflections
64 parameters
$\Delta\rho_{max}$ = 1.09 e $Å^{-3}$
$\Delta\rho_{min}$ = −0.88 e $Å^{-3}$

The site-occupancy factor of the Sc1 atom was refined freely. Because the U_{eq} parameter of atom Rb1 was larger than that of the other atoms, the site-occupancy factor of Rb1 was also refined. It converged to 1.011 (5) and was consequently fixed to unity in the final refinement. It is interesting to note that Rb atoms often present large U_{eq} values (see, for example, Picard *et al.*, 2000; Solodovnikova & Solodovnikov, 2006; Liang *et al.*, 2009; Zhao *et al.*, 2011).

Data collection: *COLLECT* (Nonius, 1998); cell refinement: *COLLECT*; data reduction: *EVALCCD* (Duisenberg *et al.*, 2003); program(s) used to solve structure: *SIR97* (Altomare *et al.*, 1999); program(s) used to refine structure: *SHELXL97* (Sheldrick, 2008); molecular graphics: *DIAMOND* (Brandenburg, 1996); software used to prepare material for publication: *SHELXL97*.

Table 1
Selected bond lengths (Å).

Rb1—S1	3.2512 (10)	Mo1—Mo2^{iii}	2.6958 (4)
Rb1—S5^{i}	3.3263 (19)	Mo1—Mo2	2.7663 (4)
Rb1—S4^{ii}	3.5475 (19)	Mo2—S1	2.4125 (10)
Rb1—S2	3.7306 (8)	Mo2—S1^{v}	2.4126 (10)
Rb1—S3	3.7554 (11)	Mo2—S2	2.4715 (11)
Sc1—S3	2.1718 (10)	Mo2—S2^{iv}	2.4715 (11)
Sc1—S4	2.7983 (3)	Mo2—Mo2^{iii}	2.6910 (8)
Sc1—S1	2.9200 (11)	Mo3—S5	2.4198 (13)
Mo1—S4	2.4336 (14)	Mo3—S3	2.4513 (10)
Mo1—S1	2.4408 (10)	Mo3—S1^{ii}	2.4577 (10)
Mo1—S1^{iii}	2.4786 (10)	Mo3—S3^{vi}	2.4641 (10)
Mo1—S3	2.5189 (10)	Mo3—S3^{vii}	2.4736 (10)
Mo1—S2	2.6065 (7)	Mo3—Mo3^{viii}	2.6783 (6)
Mo1—Mo1^{iv}	2.6658 (5)	Mo3—Mo3^{vii}	2.7393 (6)

Symmetry codes: (i) $-x+y-\frac{1}{3}, y+\frac{1}{3}, z-\frac{1}{6}$; (ii) $-x-\frac{1}{3}, -y+\frac{1}{3}, -z+\frac{1}{3}$; (iii) $-x+y-1, -x, z$; (iv) $-y, x-y+1, z$; (v) $x-y+\frac{1}{3}, -y+\frac{2}{3}, -z+\frac{1}{6}$; (vi) $x-y-\frac{1}{3}, x+\frac{1}{3}, -z+\frac{1}{3}$; (vii) $y-\frac{1}{3}, -x+y-\frac{2}{3}, -z+\frac{1}{3}$; (viii) $-x+y-1, -x-1, z$.

Intensity data were collected on the Nonius KappaCCD X-ray diffactometer system of the 'Centre de diffractométrie de l'Université de Rennes I' (http://www.cdifx.univ-rennes1.fr).

Supplementary data for this paper are available from the IUCr electronic archives (Reference: FN3104). Services for accessing these data are described at the back of the journal.

References

Altomare, A., Burla, M. C., Camalli, M., Cascarano, G. L., Giacovazzo, C., Guagliardi, A., Moliterni, A. G. G., Polidori, G. & Spagna, R. (1999). *J. Appl. Cryst.* **32**, 115–119.

Brandenburg, K. (1996). *DIAMOND*. University of Bonn, Germany.

Duisenberg, A. J. M., Kroon-Batenburg, L. M. J. & Schreurs, A. M. M. (2003). *J. Appl. Cryst.* **36**, 220–229.

Gougeon, P., Potel, M. & Sergent, M. (1989). *Acta Cryst.* C**45**, 1285–1287.

Grüttner, A., Yvon, K., Chevrel, R., Potel, M., Sergent, M. & Seeber, B. (1979). *Acta Cryst.* B**35**, 285–292.

Landrum, G. A. (1997). *YAeHMOP* (*Yet Another Extended Hückel Molecular Orbital Package*). Cornell University, Ithaca, New York, USA.

Liang, Z.-H., Tang, K.-B., Chen, Q.-W. & Zheng, H.-G. (2009). *Acta Cryst.* E**65**, i44.

Meulenaer, J. de & Tompa, H. (1965). *Acta Cryst.* **19**, 1014–1018.

Nonius (1998). *COLLECT*. Nonius BV, Delft, The Netherlands.

Picard, S., Gougeon, P. & Potel, M. (2002). *Acta Cryst.* E**58**, i12–i14.

Picard, S., Saillard, J.-Y., Gougeon, P., Noel, H. & Potel, M. (2000). *J. Solid State Chem.* **155**, 417–426.

Picard, S., Salloum, D., Gougeon, P. & Potel, M. (2004). *Acta Cryst.* C**60**, i61–i62.

Potel, M., Chevrel, R. & Sergent, M. (1981). *Acta Cryst.* B**37**, 1007–1010.

Salloum, D., Gougeon, P., Roisnel, T. & Potel, M. (2004). *J. Alloys Compd*, **383**, 57–62.

Schäfer, H. & von Schnering, H. G. (1964). *Angew. Chem.* **76**, 833–845.

Sheldrick, G. M. (2008). *Acta Cryst.* A**64**, 112–122.

Solodovnikova, Z. A. & Solodovnikov, S. F. (2006). *Acta Cryst.* C**62**, i53–i56.

Zhao, D., Li, F. F., Qiu, S., Jiao, J. & Ren, J. (2011). *Acta Cryst.* E**67**, i32.